Nuclear Safety
NEA/CSNI/R(2016)6/VOL2
February 2016
www.oecd-nea.org

Reactivity Initiated Accident (RIA) Fuel Codes Benchmark Phase-II

Volume 2:
Task No. 1 Specifications

OECD
BETTER POLICIES FOR BETTER LIVES

NEA
NUCLEAR ENERGY AGENCY

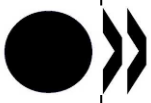

Organisation de Coopération et de Développement Économiques
Organisation for Economic Co-operation and Development

English text only

NUCLEAR ENERGY AGENCY
COMMITTEE ON THE SAFETY OF NUCLEAR INSTALLATIONS

Reactivity-Initiated Accident Fuel-Code Benchmark Phase II

Volume 2:
Task N°. 1 Specifications

NEA/CSNI/R(2016)6/VOL2
Unclassified
English text only

ORGANISATION FOR ECONOMIC CO-OPERATION AND DEVELOPMENT

The OECD is a unique forum where the governments of 34 democracies work together to address the economic, social and environmental challenges of globalisation. The OECD is also at the forefront of efforts to understand and to help governments respond to new developments and concerns, such as corporate governance, the information economy and the challenges of an ageing population. The Organisation provides a setting where governments can compare policy experiences, seek answers to common problems, identify good practice and work to co-ordinate domestic and international policies.

The OECD member countries are: Australia, Austria, Belgium, Canada, Chile, the Czech Republic, Denmark, Estonia, Finland, France, Germany, Greece, Hungary, Iceland, Ireland, Israel, Italy, Japan, Luxembourg, Mexico, the Netherlands, New Zealand, Norway, Poland, Portugal, the Republic of Korea, the Slovak Republic, Slovenia, Spain, Sweden, Switzerland, Turkey, the United Kingdom and the United States. The European Commission takes part in the work of the OECD.

OECD Publishing disseminates widely the results of the Organisation's statistics gathering and research on economic, social and environmental issues, as well as the conventions, guidelines and standards agreed by its members.

NUCLEAR ENERGY AGENCY

The OECD Nuclear Energy Agency (NEA) was established on 1 February 1958. Current NEA membership consists of 31 countries: Australia, Austria, Belgium, Canada, the Czech Republic, Denmark, Finland, France, Germany, Greece, Hungary, Iceland, Ireland, Italy, Japan, Korea, Luxembourg, Mexico, the Netherlands, Norway, Poland, Portugal, Russia, the Slovak Republic, Slovenia, Spain, Sweden, Switzerland, Turkey, the United Kingdom and the United States. The European Commission also takes part in the work of the Agency.

The mission of the NEA is:

- to assist its member countries in maintaining and further developing, through international co-operation, the scientific, technological and legal bases required for a safe, environmentally friendly and economical use of nuclear energy for peaceful purposes;
- to provide authoritative assessments and to forge common understandings on key issues, as input to government decisions on nuclear energy policy and to broader OECD policy analyses in areas such as energy and sustainable development.

Specific areas of competence of the NEA include the safety and regulation of nuclear activities, radioactive waste management, radiological protection, nuclear science, economic and technical analyses of the nuclear fuel cycle, nuclear law and liability, and public information.

The NEA Data Bank provides nuclear data and computer program services for participating countries. In these and related tasks, the NEA works in close collaboration with the International Atomic Energy Agency in Vienna, with which it has a Co-operation Agreement, as well as with other international organisations in the nuclear field.

COMMITTEE ON THE SAFETY OF NUCLEAR INSTALLATIONS

The NEA Committee on the Safety of Nuclear Installations (CSNI) is an international committee made up of senior scientists and engineers with broad responsibilities for safety technology and research programmes, as well as representatives from regulatory authorities. It was created in 1973 to develop and co-ordinate the activities of the NEA concerning the technical aspects of the design, construction and operation of nuclear installations insofar as they affect the safety of such installations.

The committee's purpose is to foster international co-operation in nuclear safety among NEA member countries. The main tasks of the CSNI are to exchange technical information and to promote collaboration between research, development, engineering and regulatory organisations; to review operating experience and the state of knowledge on selected topics of nuclear safety technology and safety assessment; to initiate and conduct programmes to overcome discrepancies, develop improvements and reach consensus on technical issues; and to promote the co-ordination of work that serves to maintain competence in nuclear safety matters, including the establishment of joint undertakings.

The priority of the CSNI is on the safety of nuclear installations and the design and construction of new reactors and installations. For advanced reactor designs, the committee provides a forum for improving safety-related knowledge and a vehicle for joint research.

In implementing its programme, the CSNI establishes co-operative mechanisms with the NEA Committee on Nuclear Regulatory Activities (CNRA), which is responsible for issues concerning the regulation, licensing and inspection of nuclear installations with regard to safety. It also co-operates with other NEA Standing Technical Committees, as well as with key international organisations such as the International Atomic Energy Agency (IAEA), on matters of common interest.

ACKNOWLEDGEMENTS

This report is prepared by the Reactivity initiated accident (RIA) Benchmark Phase-II Task Group of the Working Group of Fuel Safety (WGFS).

Special thanks go to Olivier Marchand (IRSN, France), Jinzhao Zhang (TRACTEBEL, Belgium) and Marco Cherubini (NINE, Italy) for preparing benchmark specifications and drafting the report. Vincent Georgenthum (IRSN, France) and Patrick Raynaud (NRC, USA) contributed also significantly to the preparation of the benchmark specifications. Luis Enrique Herranz (CIEMAT, Spain), Lars Olof Jernkvist (QUANTUM TECHNOLOGIES, Sweden), and Jan Klouzal (UJV, Czech Republic) reviewed the report and provided valuable comments.

LIST OF ABBREVIATIONS AND ACRONYMS

BWR	Boiling-water reactor
CABRI	Test reactor in France
CIEMAT	Centro de Investigaciones Energéticas, Medioambientales y Tecnológicas (Spain)
CSN	Consejo de Seguridad Nuclear (Spain)
CSNI	Committee on the Safety of Nuclear Installations (OECD/NEA)
CZP	Cold Zero Power
DNB	Departure from nucleate boiling
FGR	Fission-gas release
FWHM	Full width at half maximum
GRS	Gesellschaft für anlagen- und reaktorsicherheit (Germany)
HZP	Hot Zero Power
INL	Idaho National Laboratory (United States)
IRSN	Institut de radioprotection et de sûreté nucléaire (France)
JAEA	Japan Atomic Energy Agency
KINS	Korean Institute of Nuclear Safety
MOX	Mixed-oxide fuel (U and Pu)
MTA EK	Centre of Energy Research, Hungarian Academy of Sciences
NEA	Nuclear Energy Agency (OECD)
NINE	Nuclear and INdustrial Engineering (Italy)
NRC	Nuclear Regulatory Commission (United States)
NSRR	Nuclear safety research reactor (Japan)
OECD	Organisation for Economic Co-operation and Development
PCMI	Pellet cladding mechanical interaction
PWR	Pressurised-water reactor
RIA	Reactivity initiated accident
SSM	Strålsäkerhetsmyndigheten (Swedish Radiation Safety Authority)
TRACTEBEL	Tractebel engineering (ENGIE)
TSO	Technical support organisation
TUV	Technischer Überwachungsverein (Germany)
UJV	Nuclear research institute (Czech Republic), ÚJV Řež
VTT	Valtion Teknillinen Tutkimuskeskus/Technical Research Centre of Finland
WGFS	Working group on fuel safety (a CSNI working group)
xD	x-dimensional (where x is for 1.5, 2 and 3)

TABLE OF CONTENTS

1. INTRODUCTION

Reactivity-initiated accident (RIA) fuel rod codes have been developed for a significant period of time and validated against their own available database. However, the high complexity of the scenarios dealt with has resulted in a number of different models and assumptions adopted by code developers; additionally, data bases used to develop and validate codes have been different depending on the availability of the results of some experimental programmes. This diversity makes it difficult to find the source of estimates discrepancies, when this occurs.

A technical workshop on "Nuclear Fuel Behaviour during Reactivity Initiated Accidents" was organized by the OECD/NEA in September 2009. A major highlight from the session devoted to RIA safety criteria was that RIA fuel rod codes are now widely used, within the industry as well as the technical safety organizations (TSOs), in the process of setting up and assessing revised safety criteria for the RIA design basis accident. This turns mastering the use of these codes into an outstanding milestone, particularly in safety analyses. To achieve that, a thorough understanding of the codes predictability is mandatory.

As a conclusion of the workshop, it was recommended that a benchmark (RIA benchmark Phase-I) between these codes be organized in order to give a sound basis for their comparison and assessment. This recommendation was endorsed by the Working Group on Fuel Safety.

The main conclusions of this RIA benchmark Phase-I are the following [1]:

- With respect to the thermal behaviour, the differences in the evaluation of fuel temperatures remained limited, although significant in some cases. The situation was very different for the cladding temperatures that exhibited considerable scatter, in particular for the cases when water boiling occurred.
- With respect to mechanical behaviour, the parameter of largest interest was the cladding hoop strain because failure during RIA transient results from the formation of longitudinal cracks. When compared to the results of an experiment that involved only PCMI, the predictions from the different participants appeared acceptable even though there was a factor of 2 between the highest and the lowest calculations. The conclusion was not so favourable for cases where water boiling had been predicted to appear: a factor of 10 for the hoop strain between the calculations was exhibited. Other mechanical results compared during the RIA benchmark Phase-I were fuel stack and cladding elongations. The scatter remained limited for the fuel stack elongation, but the cladding elongation was found to be much more difficult to evaluate.
- The fission gas release evaluations were also compared. The ratio of the maximum to the minimum values appeared to be roughly 2, which is considered to be relatively moderate given the complexity of fission gas release processes.
- Failure predictions, which may be considered as the ultimate goal of fuel code dedicated to the behaviour under RIA conditions, were compared: it appears that the failure/no failure predictions are fairly consistent between the different codes and with experimental results. However, when

assessing the code qualification, one should rather look at predictions in terms of enthalpy at failure because it is a parameter that may vary significantly between different predictions (and is also of interest in practical reactor applications). In the frame of this RIA benchmark Phase-I the failure prediction levels among the different codes were within a +/- 50% range. A detailed and complete RIA benchmark Phase-I specification was prepared in order to assure as much as possible the comparability of the calculation results submitted.

As a conclusion of the RIA benchmark Phase-I, it was recommended to launch a second phase exercise with the following specific guidelines:

- The emphasis should be put on deeper understanding of the differences in modelling of the different codes; in particular, looking for simpler cases than those used in the first exercise was expected to reveal the main reasons for the observed large scatter in some conditions such as coolant boiling.
- Due to the large scatter between the calculations that was shown in the RIA benchmark Phase-I, it appears that an assessment of the uncertainty of the results should be performed for the different codes. This should be based on a well-established and shared methodology. This also entailed performing a sensitivity study of results to input parameters to assess the impact of initial state of the rod on the final outcome of the power pulse.

The Working Group on Fuel Safety endorsed these recommendations and a second phase of the RIA fuel-rod-code benchmark (RIA benchmark Phase-II) was launched early in 2014. This RIA benchmark Phase-II has been organized as two complementary activities:

- The first activity is to compare the results of different simulations on simplified cases in order to provide additional bases for understanding the differences in modelling of the concerned phenomena.
- The second activity is focused on the assessment of the uncertainty of the results. In particular, the impact of the initial states and key models on the results of the transient are to be investigated.

The Volume 1 of the report provides a summary and documents the conclusions and recommendations from the first activity.

The present Volume 2 of the report provides first activity specifications that were prepared in order to ensure as much as possible the comparability of the calculation results submitted.

The complete set of solutions provided by all the participants are compiled in Volume 3.

2. FIRST ACTIVITY: SIMPLIFIED CASES

2.1 Objectives

The objective of this first part of the RIA benchmark Phase-II is to compare the results of different simulations on simplified Cases, in order to better understand the differences in modelling of the concerned specific phenomena.

Ten Cases were defined with an increasing degree of complexity to assess the different phenomena step by step.

The first Case is mainly devoted to the thermal behaviour, the second and third Cases are focused on the thermo-mechanical behaviour, and in the last five Cases the thermal-hydraulics behaviour aspect is added.

2.2 Modelling recommendations

For each code, it is recommended to use the standard options for all models except for the failure model, fuel relocation model, and high temperature cladding oxidation model, which must be disabled (considering the proposed problems). In one Case thermal and thermal-mechanical properties/models for clad and fuel should be imposed as close as possible to those of FRAPTRAN.

2.3 Description of the cases

2.3.1 General design

To limit the differences linked to the initial state of the fuel, the Cases are limited to a fresh 17x17 PWR type fuel rod as described in Figure 2-1.

In all Cases, starting from ambient conditions, a stabilisation phase is simulated before the real transient phase in order to reach the foreseen initial state of the rod.

Two different values for the clad inner radius are used to impose the presence or absence of an initial gap between the fuel and the clad. In most of the Cases, the fuel and the clad are considered bonded (no slipping between the fuel and the clad is assumed) except for one Case where perfect slipping between the fuel and the clad is assumed as contact condition.

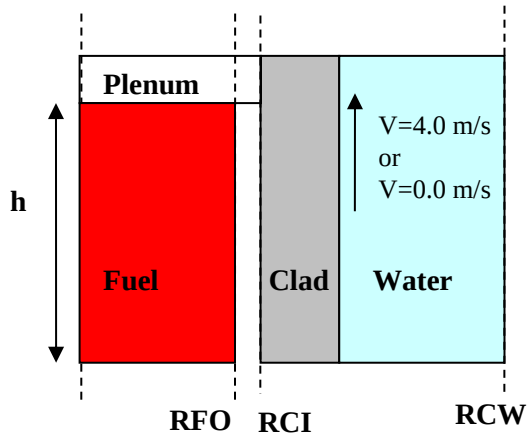

Fuel outer radius (RFO) = 4.13 mm
Clad inner radius (RCI) = 4.13 or 4.18 mm
Clad thickness = 570 µm
Water canal radius (RCW) = 7.5 mm
Upper plenum volume =2 cm^3
Fuel height (h) = 10 cm

Figure 2-1: Rod design

2.3.2 Fuel rod characteristics

The geometry parameters for the fuel rod are related to room temperature (T_{room}), that is 20°C.

Fuel characteristics

- Fuel pellet composition: UO_2 with 4.1% enrichment,
- Fuel pellet height: 1 cm,
- Fuel pellet diameters: 8.26 mm (dishing and chamfer are not taken into account),
- Fuel theoretical density: 10970 kg/m^3, (at 20°C)
- Fuel porosity: 4%,
- Fuel grain size: 5 µm,
- Fissile column height: 10 cm,
- Upper plenum: 2 cm^3,
- Spring: Not considered.

Clad characteristics

- Cladding material: Standard Zircaloy-4,
- Clad thickness: 0.57 mm,
- Clad outer diameter: 9.4 or 9.5 mm (see case description).

Gap characteristics

- Filling gas: Helium, pressure= 20 or 50 bar at room temperature (see case description),
- Fuel roughness: 0.1 µm,
- Clad roughness: 0.1 µm.

2.3.3 Coolant characteristics during transient

Depending on the case (see case description), the thermal-hydraulics conditions during transient could be:

- water coolant in nominal PWR conditions (coolant inlet conditions: P_{cool}=155 bar, T_{cool}=280°C at V_{cool}=4 m/s) with a channel radius equal to 7.5 mm (referred as "**PWR conditions**"),
- water coolant in BWR cold zero power (CZP) conditions (coolant inlet conditions: P_{cool}=1 bar, T_{cool}=20°C at V_{cool}=0.0 m/s) with a channel radius equal to 7.5 mm (referred as "**BWR conditions**"),
- imposed coolant bulk temperature (T_{bulk}=300°C during the first 5 seconds, then T_{bulk}=T_{cool}=280°C till the end of transient); imposed clad to coolant heat transfer coefficient (H_{trans}=4000 W/m^2/K during the first 5 seconds, then H_{trans}=H_{steady}=40000 W/m^2/K till the end of transient) and external pressure at 155 bar (P_{cool}) with a channel radius equal to 7.5 mm (referred as "**imposed conditions**"),
- imposed external clad temperature at 280°C (T_{cool}) and external pressure at 155 bar (P_{cool}) (referred as "**fixed conditions**"). In that case, the coolant conditions (temperature and flow rate) have no impact on the fuel behaviour.

2.3.4 Pulse characteristics and power profile

The pulse will start from zero power and it is considered to have a triangular shape, with 30 ms of Full Width at Half Maximum (FWHM) and two values for the rod maximal power in the fuel PMax (see Figure 2-5) is considered:

- a low value to avoid DNB occurrence,
- a high value to provoke DNB occurrence.

For PWR Cases (all cases, except Case No. 6 and Case No. 7) the low value will be 4.10^5 W (leading to an injected energy of 50.82 cal/g) and the high value will be 1.10^6 W (leading to an injected energy of 127.06 cal/g).

For BWR cases (Case No. 6 and Case No. 7) the low value will be 3.10^5 W (leading to an injected energy of 38.12 cal/g) and the high value will be 1.10^6 W (leading to an injected energy of 127.06 cal/g).

The whole power will be injected in UO_2 and no contribution will be released in the clad and in the water.

The axial and radial profiles in the fuel are supposed to be flat.

2.3.5 Initial conditions

For all calculations except for Case No. 9, the fuel and cladding will be initialized at room temperature (T_{room}) at zero power and the coolant will be initialized at T_{room}, P_{room} (1 bar) and V_{cool} (depending on the case).

For Case No. 9, coolant bulk temperature will be fixed at T_{room} and the clad to coolant heat transfer coefficient will be fixed at HCW_{steady} (40000 $W/m^2/K$). Coolant pressure will be initialized at P_{room} (1 bar).

2.3.6 Transient conditions

In order to reach the desired conditions before the pulse, the coolant conditions will be increased from the initial conditions to the conditions corresponding to the case ("fixed conditions", "imposed conditions", "PWR conditions" or "BWR conditions"). Figure 2-3, Figure 2-4, Figure 2-5, Figure 2-6, and Figure 2-7 give the evolution to be imposed and parameters are given in Table 2-1.

Time parameters	t_0	t_1	t_2	t_3	t_4	t_5
Value (s)	**0.000**	**50.000**	**100.000**	**100.060**	**105.000**	**200.000**

Table 2-1: time parameters for transient conditions

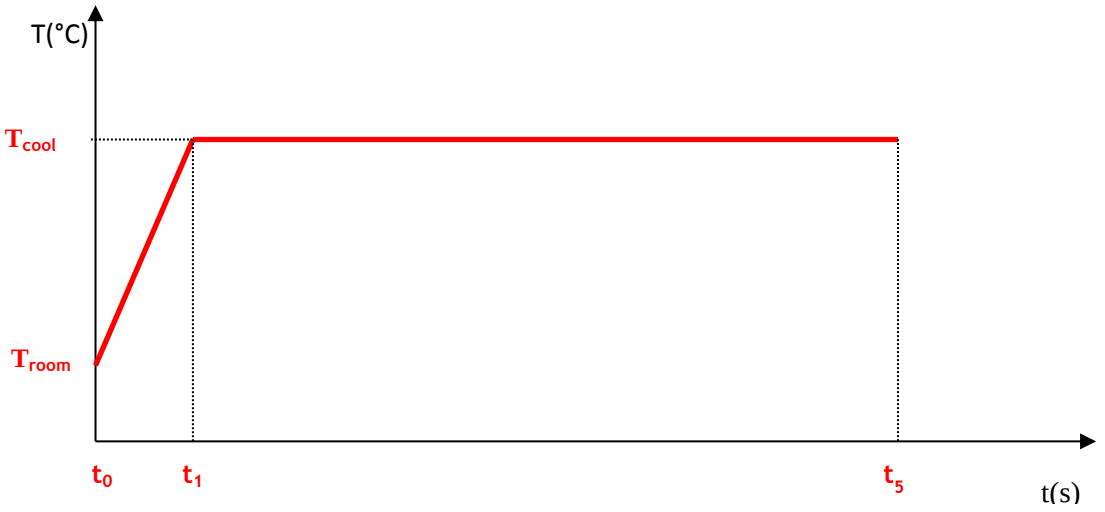

Figure 2-2: Inlet coolant temperature evolution

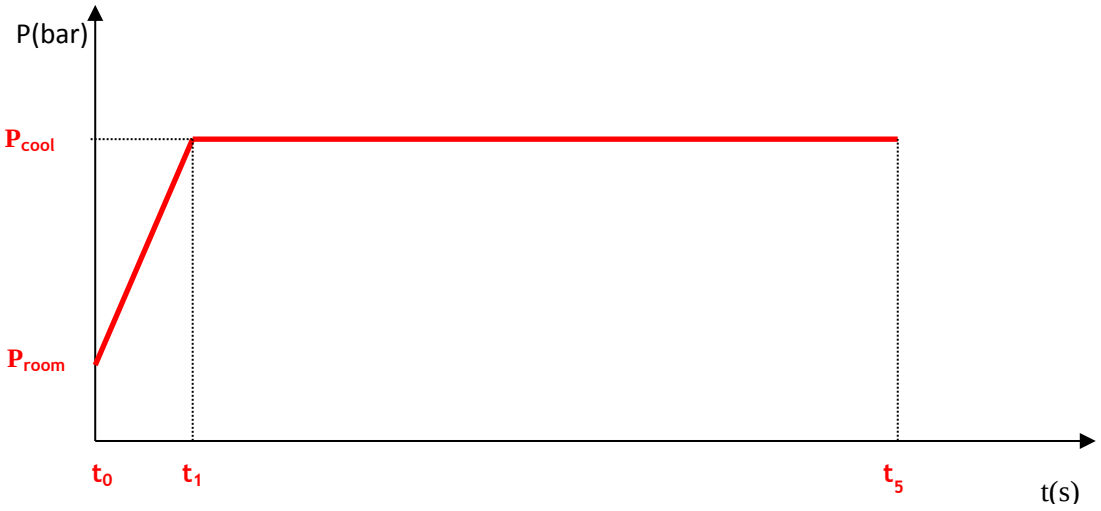

Figure 2-3: Inlet coolant pressure evolution

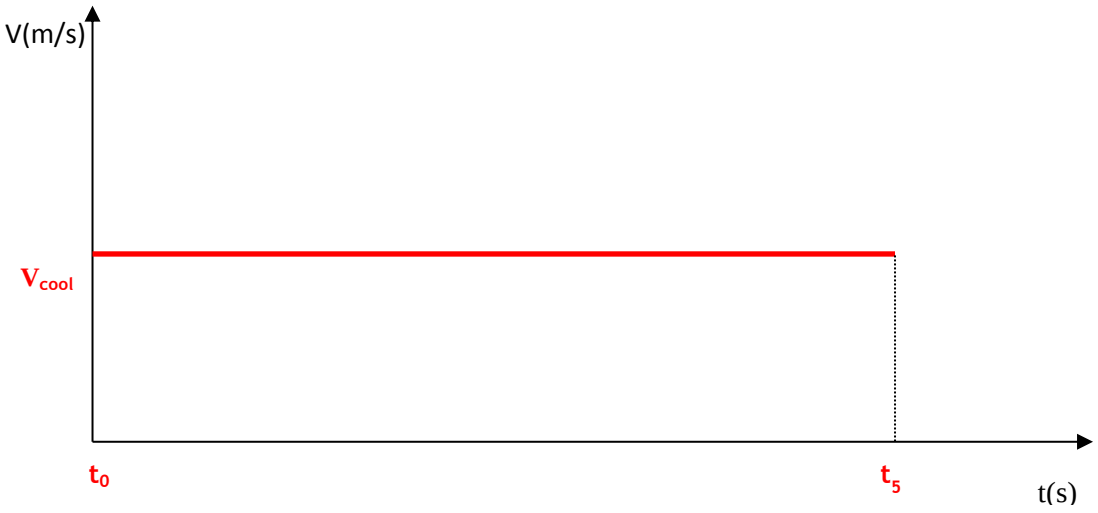

Figure 2-4: Inlet coolant velocity evolution

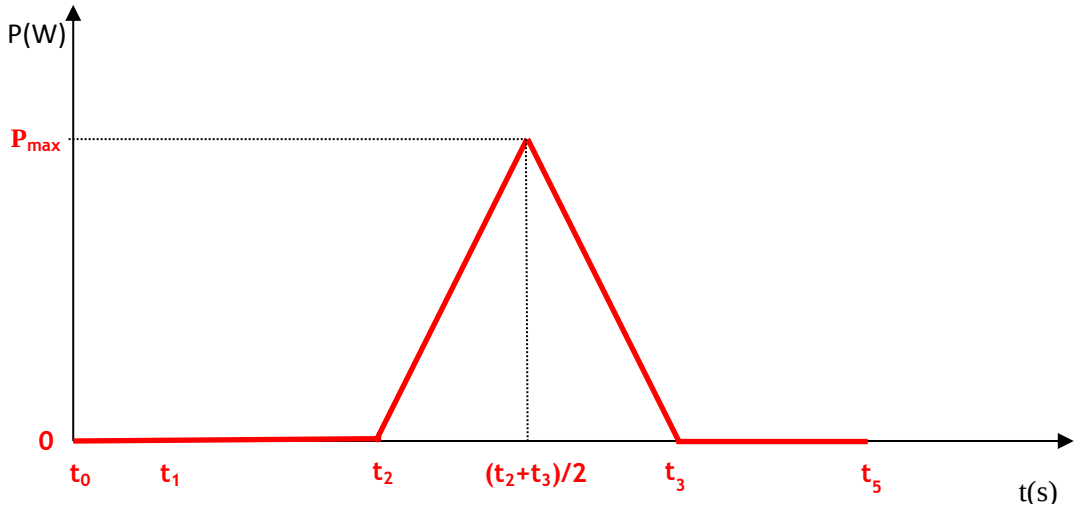

Figure 2-5: Rod power evolution

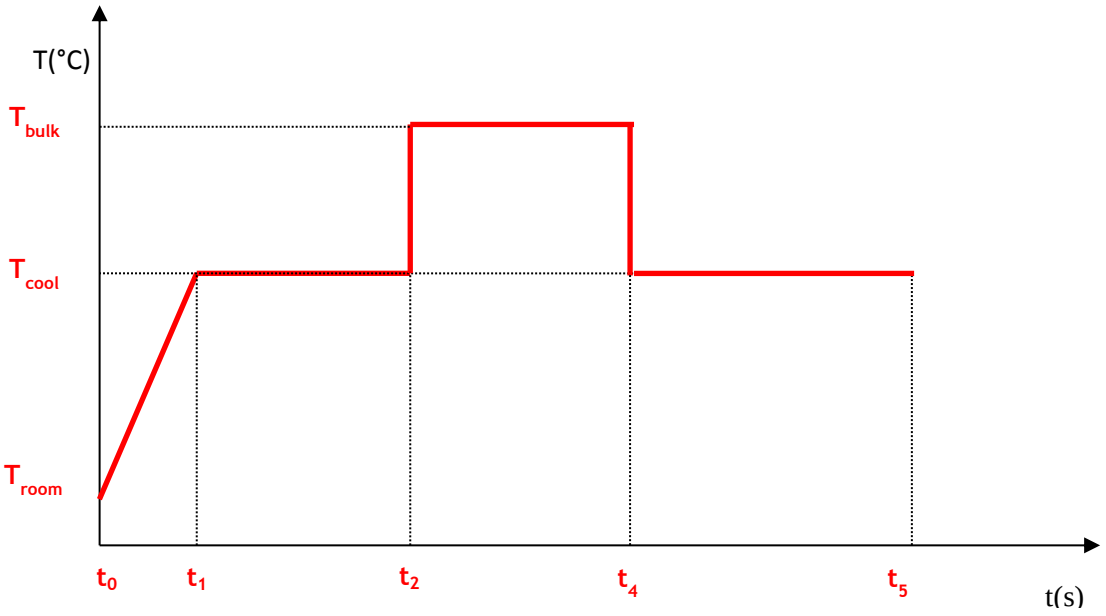

Figure 2-6: Bulk temperature evolution

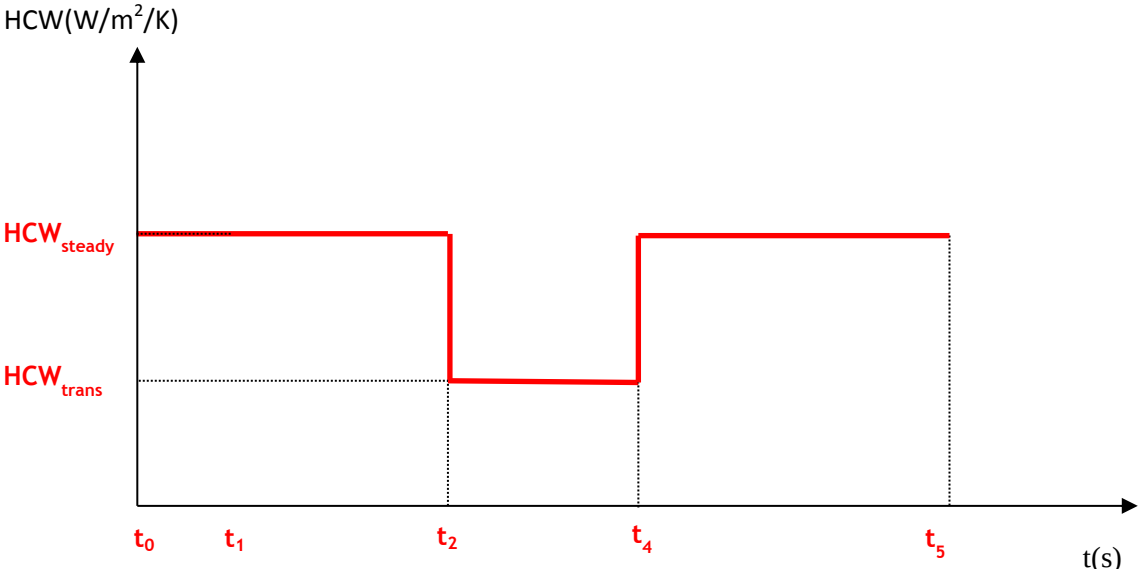

Figure 2-7: Coolant to clad heat transfer coefficient evolution

2.3.7 Thermal assessment (Case No. 1)

The clad has a lower diameter than the standard ones of 17x17 PWR type in order to close the initial pellet/cladding gap (clad inner diameter = 8.26 mm). The fuel is supposed to be bonded to the clad (no slipping between the fuel and the clad is assumed).

The coolant characteristics are "fixed conditions", the internal rod pressure is 20 bar at 20°C and the maximal power is 1.10^6 W.

2.3.8 Thermal-mechanical assessment (Case No. 2, Case No. 3 and Case No. 10)

Three cases to assess the mechanical behaviour are defined. We consider in these three cases an initial gap between fuel and cladding of 50 µm (inner clad diameter = 8.36 mm). When the fuel-clad gap is closed, the fuel is considered bonded to the cladding in the Case No. 2 (friction=1) and Case No. 10 (no slipping assumed) and with a perfect slipping (friction=0) in the Case No. 3.

The coolant characteristics are "fixed conditions", the internal rod pressure is 20 bar at 20°C and the maximal power is 1.10^6 W.

In Case No. 10, the thermal and thermal-mechanical clad and fuel behaviours will be imposed for each code as presented in appendix 1 (each participant will try to impose the same properties as in FRAPTRAN calculation). In Case No. 2 and Case No. 3, the standard models are used.

2.3.9 BWR thermal-hydraulics assessment (Case No. 6 and Case No. 7)

The clad has a lower diameter than the standard ones of 17x17 PWR type in order to close the initial pellet/cladding gap (clad inner diameter = 8.26 mm). The fuel is supposed to be bonded to the clad (no slipping assumed).

The coolant characteristics are in "BWR conditions", the internal rod pressure is 20 bar at 20°C.

In Case No. 6, maximal power is decreased to 3.10^5 W in order to avoid the boiling crisis. In Case No. 7, maximal power is 1.10^6 W in order to reach the boiling crisis.

2.3.10 PWR thermal-hydraulics assessment (Case No. 4, Case No. 5, Case No. 8 and Case No. 9)

The clad has a smaller diameter than the standard ones of 17x17 PWR type in order to close the initial pellet/cladding gap (clad inner diameter = 8.26 mm). The fuel is supposed to be bonded to the clad (no slipping assumed).

For Case No. 4, Case No. 5 and Case No. 8, the coolant characteristics are in "PWR condition" and for Case No. 9 the coolant characteristics are in "imposed conditions".

In Case No. 4, maximal power is decreased to 4.10^5 W in order to avoid the boiling crisis. In Case No. 5, Case No. 8 and Case No. 9, maximal power is 1.10^6 W in order to reach the boiling crisis.

In Case No. 8, the helium pressure is increased to 50 bar (at 20°C) to enhance the possible post-boiling crisis strain; for all other cases (Case No. 4, Case No. 5 and Case No. 9) the internal rod pressure is 20 bar at 20°C.

2.3.11 Synthesis of specified cases

		Geometry		Contact Conditions		Thermal Mechanical Models		Thermal Hydraulic Conditions				Pmax		Helium Pressure	
		No gap	Open gap	No Slipping	Slipping	Standard	Imposed	Fixed	PWR	BWR	Imposed	Low	High	Low	High
Thermal	Case No. 1	X		X		X		X					X	X	
Mechanical	Case No. 2		X	X		X		X					X	X	
	Case No. 3		X		X	X		X					X	X	
	Case No. 10		X	X			X	X					X	X	
Thermal Hydraulic	Case No. 6	X		X		X				X		X		X	
	Case No. 7	X		X		X				X			X	X	
	Case No. 4	X		X		X			X			X		X	
	Case No. 5	X		X		X			X				X	X	
	Case No. 8	X		X		X			X				X		X
	Case No. 9	X		X		X					X		X	X	

Table 2-2: summary of cases

2.4 Parameters to be calculated

2.4.1 List of parameters

The results to be calculated are defined in the following Table 2-3 for all cases.

Parameter	Unit	Description
EDR	cal/g	Energy Injected in the whole rodlet as a function of time
DHR	cal/g	Variation of radial average enthalpy with respect to initial conditions of the transient in the rodlet as a function of time (at z=h/2) (please note that: DHR(t=0)=0)
TFC	°C	Temperature of fuel centreline as a function of time (at z=h/2)
TFO	°C	Temperature of fuel outer surface as a function of time (at z=h/2)
TCI	°C	Temperature of clad inner surface as a function of time (at z=h/2)
TCO	°C	Temperature of clad outer surface as a function of time (at z=h/2)
ECMH	%	Clad mechanical (elastic + plastic) hoop strain at the outer part of the clad as a function of time (at z=h/2)
ECMZ	%	Clad mechanical (elastic + plastic) axial strain at the outer part of the clad as a function of time (at z=h/2)
ECTH	%	Clad total (thermal + elastic + plastic) hoop strain at the outer part of the clad as a function of time(at z=h/2)
ECTZ	%	Clad total (thermal + elastic + plastic) axial strain at the outer part of the clad as a function of time(at z=h/2)
ECT	mm	Clad total axial elongation as a function of time
EFT1	mm	Fuel column total axial elongation as a function of time
EFT2	mm	Fuel column thermal axial elongation as a function of time
SCH	MPa	Clad hoop stress at outer part of the clad as a function of time (at z=h/2)
SCZ	MPa	Clad axial stress at outer part of the clad as a function of time (at z=h/2)
RFO	mm	Fuel outer radius as a function of time (at z=h/2)
RCI	mm	Clad inner radius as a function of time (at z=h/2)

HFC	$W/m^2/K$	Fuel to clad heat transfer coefficient as a function of time (at z=h/2)
HCW	$W/m^2/K$	Clad to water heat transfer coefficient as a function of time (at z=h/2)
PG	bar	Free volume pressure as a function of time
VOL	mm^3	Free Volume as a function of time (including open porosity)

Table 2-3: list of parameters to be provided

2.4.2 File format of parameters

One formatted Excel file is expected for each case (see file task-1_case_i.xlsx).

Please note that only 5000 points per each parameter are accepted.

3. REFERENCES

[1] NEA/CSNI/R(2013)7, RIA Fuel Codes Benchmark - Volume 1, Nuclear Energy Agency, OECD, Paris, France (2013).

4. APPENDIX 1: FRAPTRAN MODELS FOR CASE NO. 10

4.1 Fuel

4.1.1 Density, densification, and swelling

Fuel density is a user-supplied input in both FRAPCON and FRAPTRAN. However, densification is also modelled in FRAPCON and passed onto FRAPTRAN through a restart file for cases with non-zero burnup.

The subroutine FUDENS calculates fuel dimensional changes due to densification of UO_2 during the first few thousand hours of water reactor operation.

The FUDENS subroutine is used in FRAPCON-3.5 and is similar to the correlation described by MATPRO. However, FUDENS is not included in FRAPTRAN because FRAPTRAN is intended for transient events occurring over a short time scale. Since densification occurs over longer time scales, it is not included in FRAPTRAN.

The subroutine FSWELL calculates fuel swelling, which is caused by the build-up of solid and gaseous fission products during irradiation. The FSWELL subroutine is only applicable to time scales on the order of minutes to hours and, therefore, not used in FRAPTRAN-1.5.

4.1.2 Thermal conductivity

The subroutine FTHCON is used to calculate the thermal conductivity of the fuel pellet.

Both FRAPCON-3.5 and FRAPTRAN-1.5 currently model urania fuel pellet thermal conductivity with the modified version of the pellet thermal conductivity model proposed by NFI (Ohira and Itagaki, 1997). The original NFI model was modified to alter the temperature-dependent portion of the burnup function in the phonon terms and change the electronic term (Lanning et al., 2005). The modified version of the NFI thermal conductivity model is presented below.

$$K_{95} = \frac{1}{A + BT + f(Bu) + (1 - 0.9\exp(-0.04Bu))\, g(Bu)\, h(T)} + \frac{E}{T^2}\exp(-F/T)$$

where

K = thermal conductivity, W/m-K
T = temperature, K
Bu = burnup, GWd/MTU
f(Bu) = effect of fission products in crystal matrix (solution)
= 0.00187 * Bu

g(Bu) = effect of irradiation defects
= 0.038 * Bu0.28
h(T) = temperature dependence of annealing on irradiation defects

$$= \frac{1}{1+396\exp(-Q/T)}$$

Q = temperature-dependent parameter ("Q/R") = 6380K
A = 0.0452 m-K/W
B = 2.46×10^{-4} m-K/W/K
C = 5.47×10^{-9} W/m-K^3
D = 2.29×10^{14} W/m-K^5
E = 3.5×10^{9} W-K/m

As applied in FRACON-3.5 and FRAPTRAN-1.5, the above model is adjusted for as-fabricated fuel density (in fraction of theoretical density [TD]) using the Lucuta recommendation for spherical-shaped pores (Lucuta et al., 1996), as follows:

$$K_d = 1.0789 * K_{95} * [d/\{1.0 + 0.5(1-d)\}]$$

where

K_d = thermal conductivity adjusted for as-fabricated fuel density, d
K_{95} = thermal conductivity for 95 percent dense fuel
d = as-fabricated fuel density

4.1.3 Heat capacity

The subroutines FCP and FENTHL are used to calculate the specific heat capacity and enthalpy of the fuel pellet, respectively. The specific heat capacity and enthalpy of nuclear fuel are modelled empirically as functions of four parameters: temperature, composition, molten fraction, and oxygen-to-metal (O/M) ratio. The same subroutine is used in FRAPCON-3.5, FRAPTRAN-1.5, and MATPRO.

Equations for the specific heat capacity and enthalpy of solid UO_2 and plutonium dioxide (PuO_2) are assumed to have the same form, but with different constants. The basic relationships are below.

$$FCP = \frac{K_1\theta^2 \exp(\theta/T)}{T^2[\exp(\theta/T)-1]^2} + K_2 T + \frac{YK_3E_D}{2RT^2}\exp(-E_D/RT)$$

$$FENTHL = \frac{K_1\theta}{\exp(\theta/T)-1} + \frac{K_2T^2}{2} + \frac{Y}{2}[K_3\exp(-E_D/RT)]$$

where

FCP = specific heat capacity (J/kg*K)
FENTHL = fuel enthalpy (J/kg)
T = temperature (K)
Y = oxygen-to-metal ratio
R = universal gas constant (8.3143 J/mol*K)
θ = the Einstein temperature (K)
E_D = activation energy for Frenkel defects (J/mol)

Constant	UO_2	Units
K_1	296.7	J/kg*K
K_2	2.43×10^{-2}	$J/kg*K^2$
K_3	8.745×10^{7}	J/kg
θ	535.285	K
E_D	1.577×10^{5}	J/mol

The constants were determined by Kerrisk and Clifton (1972) for UO_2. The specific heat capacity of UO_2 in the liquid state was determined by Leibotwitz (1971) and assumed to be valid for PuO_2 in the liquid state.

FCP_{Liquid} = 503J/kg*K

4.1.4 Emissivity

The subroutine FEMISS is used to calculate the total hemispherical fuel emissivity (emissivity integrated over all wavelengths) as a function of temperature. Fuel emissivity is defined as the ratio of radiant energy emitted from a material to that emitted by a black body at the same temperature. The subroutine FEMISS is used to calculate radiant energy transfer from fuel to cladding in conjunction with thermal conduction. Radiant energy transfer can be a significant heat transfer mechanism, depending on the gap size, temperature gradient across the gap, and plenum gas. The FEMISS subroutine used by FRAPCON-3 and FRAPTRAN is the same as the subroutine documented in MATPRO.

According to the Stefan-Boltzmann law, the total radiant power per unit area emitted by a body at temperature T is:

$$P = e\sigma T^4$$

where

P = radiant power per unit area (W/m^2)
e = total hemispherical emissivity (dimensionless)
σ = the Stefan-Boltzmann constant (5.672×10^{-8} W/m^2-K)
T = temperature (K)

The expression used in the FEMISS subroutine to describe total emissivity is:

$$e = 0.78557 + 1.5263 x 10^{-5} T$$

4.1.5 Hardness

Not modelled: a rigid pellet model is used, thus the hardness is effectively infinite.

4.1.6 Thermal expansion coefficient

The subroutine FTHEXP models dimensional changes in unirradiated fuel pellets caused by thermal expansion. The FTHEXP subcode models fuel thermal expansion as a function of temperature, fraction of

PuO_2, and the fraction of fuel which is molten. The O/M ratio is not included. When the departure from stoichiometry (O/M – 2.0) is greater than 0.2, there is clearly an effect. However, this effect is ignored in modelling thermal expansion, since typical reactor fuels only deviate less than a tenth this much from the stoichiometric composition.

The equation for thermal expansion of UO_2 is:

$$\Delta L / L_0 = K_1 T - K_2 + K_3 \exp(-E_D / kT)$$

where

$\Delta L/L_0$ = linear strain caused by thermal expansion (equal to zero at 300K - dimensionless)
T = temperature (K)
E_D = energy of formation of a defect (J)
k = Boltzmann's constant (1.38×10^{-23} J/K)

and K_1, K_2, and K_3 are constants to be determined.

Data collected by Baldock et al. (1966), Burdick and Paker (1956), Gronvold (1955), Christensen (1963), and Kempeter and Elliott (1958) were used to determine the correlation constants for UO_2 used in MATPRO. However, newer data provided by Martin (1988) and Momin et al. (1991) required the constants to be updated to improve the fit between the correlation and high-temperature data (Luscher and Geelhood, 2011). These updated constants are included in FRAPCON-3.5/FRAPTRAN-1.5 (FRAP).

Constant	**FRAP UO_2**	**Units**
K_1	9.80×10^{-6}	K^{-1}
K_2	2.61×10^{-3}	Dimensionless
K_3	3.16×10^{-1}	Dimensionless
E_D	1.32×10^{-19}	J

During melting, an expansion equal to a linear strain of 0.043 occurs. If the fuel is partially molten, the strain due to thermal expansion is given by:

$$\Delta L / L_0 = \Delta L / L_0(T_m) + 0.043 \cdot FACMOT$$

where

$\Delta L/L_0(T_m)$ = thermal expansion strain of solid fuel from equations with $T = T_m$
T_m = melting temperature of the fuel (K)
FACMOT = fraction of the fuel which is molten (dimensionless)
If FACMOT = 0.0, the fuel is all solid
If FACMOT = 1.0, the fuel is all molten

The correlation used to describe the expansion of entirely molten fuel is given by:

$$\Delta L / L_0 = \Delta L / L_0(T_m) + 0.043 + 3.6x10^{-5}\left[T - \left(T_m + \Delta T_m\right)\right]$$

The solid-to-liquid phase transition is isothermal only for pure UO_2 or pure PuO_2. For MOX, the transition occurs over a finite temperature range, denoted by ΔTm.

4.1.7 Young's modulus

Not modelled: a rigid pellet model is used, thus the Young's modulus is effectively infinite.

4.1.8 Poisson's ratio

Not modelled: a rigid pellet model is used, thus the Poisson's ratio is effectively zero.

4.1.9 Yield Strength

Not modelled: a rigid pellet model is used, thus the yield strength is effectively infinite.

4.1.10 Mechanical behaviour model

This section describes the models used to calculate fuel deformation in FRACAS-I. Models are used to calculate the fuel stack length change, fuel radial displacement, fuel crack volume, and fuel open porosity.

The fuel deformation model is based on the following assumptions.

1. The sources of fuel deformation are thermal expansion, fuel relocation, and a user input option to specify transient gaseous fuel swelling.
2. No resistance to the fuel deformation occurs.
3. Axial thermal expansion of the fuel stack is equal to thermal expansion of a line projected through the dish shoulder of the fuel pellets.
4. No creep deformation of the fuel occurs.
5. The fuel has isotropic properties.

The length change of the fuel pellet stack is assumed equal to the thermal expansion of the line projected through the shoulders of the fuel pellet dishes, as illustrated below. The length change is given by:

$$\Delta L_f = \sum_{n=1}^{N}\left[\varepsilon_T(T_{sn}) - \varepsilon_T(T_0)\right]\Delta Z_n$$

where

ΔL_f = fuel stack length change (m)
$\varepsilon_T(T)$ = thermal expansion of fuel at temperature T obtained from material properties handbook (Luscher and Geelhood, 2014) - (m/m)

T_{sn} = fuel temperature at pellet shoulder at axial node n (K)

T_o = strain free fuel reference temperature (K)
ΔZ_n = fuel stack length associated with axial node n (m)

Fuel radial displacement from thermal expansion is calculated by

$$U_F = U_T + U_C$$

where

U_F = radial displacement of fuel pellet outer surface (m)
U_T = radial displacement of fuel due to thermal expansion (m)

$$= \int_0^{r_f} \varepsilon_T[T(r)]dr$$

ε_T = thermal expansion of fuel (m/m)
r_f = as-fabricated fuel pellet outer radius (m)
T(r) = fuel temperature at radial coordinate r (K)
U_C = the additional radial displacement at pellet-pellet interface due to "hourglassing" of the fuel pellets

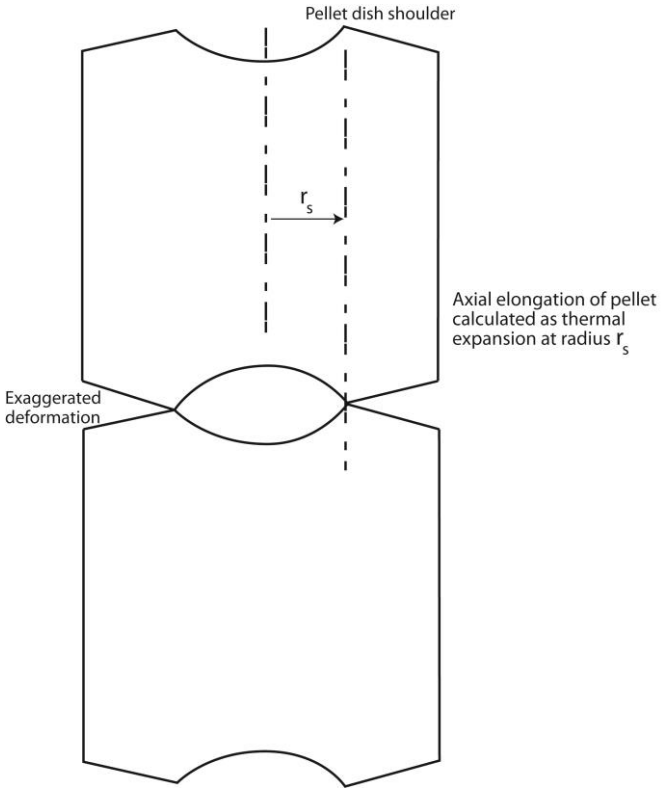

Figure 4-1: Axial thermal expansion using FRACAS-I

The additional radial displacement, UC, is assumed to occur at the ends of the fuel pellets and affect both fuel-cladding mechanical interaction and fuel-cladding heat transfer. The same gap is used for both mechanical and thermal calculations.

The additional radial displacement is calculated by the expression

$$
\begin{aligned}
U_c &= 0.0025 r_f && P_I = 0 \\
U_c &= 0.0025 r_f \left(1 - \frac{P_I}{3.45\times10^7}\right) && 0 < P_I < 3.45\times10^7 \\
U_c &= 0 && P_I \geq 3.45\times10^7
\end{aligned}
$$

where

P_I is fuel-cladding interfacial pressure (N/m^2).

Once the fuel-cladding gap is closed, the cladding is assumed to follow the fuel dimensional changes from fuel thermal expansion and fuel melting. This assumes that there is little fuel creep or compliance. This may overpredict fuel-cladding mechanical interaction strain for some transients with high fuel centreline temperatures (> 2000°C) because some of the expansion may result in some fraction of dish filling, which would not contribute to fuel-cladding mechanical interaction strains. These assumptions may also lead to the code overpredicting cladding strains for slow transients on the order of minutes that can also be adequately predicted with steady-state fuel performance codes.

Fuel pellet cracking, beginning with the initial ascension to power, promotes an outward radial relocation (movement) of the pellet fragments that causes additional gap closure. A simplified relocation model is provided in FRAPTRAN that is based on the model used in FRAPCON-3 (Lanning et al., 1997). The model used in FRAPTRAN is as follows:

if burnup = 0, relocation = 0.30* gap
if burnup > 0, relocation = 0.45* gap

where

gap is the as-fabricated radial fuel-cladding gap.

Because of the rapid nature of transients, no recovery of the relocation is allowed by FRAPTRAN, whereas FRAPCON-3 does allow some recovery under some conditions. The application of this model to fuel rods with diametral cold gaps of 0.005 inch or less may result in premature gap closure, fuel-cladding mechanical interaction, and underpredicted fuel temperatures.

If FRAPTRAN is initialized using a FRAPCON-3 file, then relocation is included in the burnup-dependent radial dimensions and the above model is bypassed.

4.1.11 Permeability (gission gas release model)

FRAPTRAN has a model to calculate the transient release of fission gases as a function of temperature. FRAPTRAN also has a user input option to specify the fission gas release as a function of time.

The transient release of fission gas is highly dependent on the location of the gas in the fuel pellet, both radially, and in each radial node the location (in the grains versus on the grain boundaries) of the

gas. Because of this, the transient gas release model in FRAPTRAN may only be used if initialized with a FRAPCON-3 burnup initialization file. In addition, FRAPCON-3 must have been run with the FRAPFGR model (ngasmod=3 in FRAPCON-3). This model has been developed specifically to predict the location of fission gas within the pellets. This transient release model is described below:

- All grain boundary gas for a given radial node is released when the temperature exceeds 2000°F (1093°C).
- All gas in the restructured grains (matrix) of the high burnup structure for a given radial node is released when the temperature exceeds 3300°F (1816°C).
- Five percent of the gas in the unrestructured grains (matrix) for a given radial node is released when the temperature exceeds 3300°F (1816°C).

This release model was developed to predict the measured release data from RIA experimental tests in CABRI and NSRR. (See data comparisons in Geelhood and Luscher (2014b).

A user input option is available (MODEL data block) to specify the fission gas release to the fuel-cladding gap and rod plenum during a transient. The user specifies the rod-average fractional fission gas release as a function of time during the transient. Rod-average burnup is used to calculate the rod-average fission gas production which is available to be released. The released fission gas affects the gas pressure and composition, which in turn affects the transient thermal and mechanical calculations.

4.2 Cladding

4.2.1 Density

The density of the cladding is assumed to be equal to the theoretical density of Zircaloy at room temperature (6.56 g/cm^3). The exception is in the subroutines used to calculate ECR, where the cladding density is assumed equal to the theoretical density of pure zirconium at 1200°C (6.49 g/cm^3).

4.2.2 Thermal conductivity of zircaloy

The subroutine CTHCON is used to calculate cladding thermal conductivity, which is required for accurate predictions of fuel temperature. The thermal conductivity of the cladding is primarily a function of temperature. Other characteristics, such as residual stress levels, crystal orientation, and minor composition differences, may have secondary effects on thermal conductivity. The correlation used in CTCHCON to calculate cladding thermal conductivity is the same in MATPRO, FRAPCON-3.5, and FRAPTRAN-1.5. This correlation is applied to Zircaloy-2, -4, ZIRLO, Optimized ZIRLO, and M5.

Considering only temperature as the defining parameter, the thermal conductivity of Zircaloy for temperatures less than 2098K is described by CTHCON as follows, with the uncertainty also provided.

$$k = 7.51 + 2.09x10^{-2}\,T - 1.45x10^{-5}\,T^2 + 7.67x10^{-9}\,T^3$$
$$\sigma_k = 1.01$$

For temperatures greater than or equal to 2098K, the thermal conductivity and uncertainty are given below, respectively.

$$k = 36$$
$$\sigma_k = 5$$

where

k = thermal conductivity of Zircaloy (W/m* K)
T = temperature (K)
σ_k = standard deviation (W/m*K)

4.2.3 Thermal conductivity of oxide

The ZOTCON subroutine calculates the thermal conductivity of the zirconium oxide layer that forms on zirconium alloys. Cladding temperature is the only parameter used to calculate zirconium oxide thermal conductivity. The correlation used in FRAPCON-3.5 and FRAPTRAN-1.5 is based on measurements obtained by Kingery (1954) from fully dense and porous (87 percent TD) zirconium oxides.

$$K_{FRAP} = 1.9599 - T*(2.41x10^{-4} - T*(6.43x10^{-7} - T*1.946x10^{-10}))$$

4.2.4 Heat capacity

The specific heat subcode, CCP, determines the true specific heat at constant pressures for cladding. Specific heat calculations are based on interpolation of measured data. The correlation in FRAPCON-3.5, FRAPTRAN-1.5, and MATPRO is applicable to Zircaloy-2, Zircaloy-4, ZIRLO, Optimized ZIRLO, and M5 alloys.

The CCP subcode requires temperature as an input to calculate specific heat. For the alpha phase of the Zircaloy alloys (temperature less than 1090K), CCP returns linear interpolations. These data points are based on precise data taken by Brooks and Stansbury (1966) with a Zircaloy-2 sample that had been vacuum-annealed at 1075K to remove hydrogen, which would have otherwise affected the measurement.

The standard errors associated with this interpolation technique differ between MATPRO and FRAPCON-3.5/FRAPTRAN-1.5. In MATPRO, the standard error of the CCP interpolation was based on 90 points in the Brooks and Stansbury (1966) database and was found to be temperature dependent. For the 57 data points between 300 and 800K, the standard error is 1.1 J/kg*K. Between 800 and 1090K, it is 2.8J/kg*K. The FRAPCON-3.5/FRAPTRAN-1.5 codes assume a standard error of 10 J/kg*K below 1090K.

For temperatures from 1090 to 1300K (where Brooks and Stansbury do not report results), values of specific heat proposed by Deem and Eldridge (1967) are adopted. The Deem and Eldridge (1967) values are based on measurements of enthalpy and temperature which provide considerably less precise specific heat data than the results of Brooks and Stansbury (1966).

As a result, the MATPRO standard error estimated from the Deem and Eldridge (1967) data in the region of 1090 through 1310K is 10.7 J/kg*K. This standard error is a measure only of the precision of the fit, since only a single data source is used. The standard error in FRAPCON 3.5/FRAPTRAN-1.5 is assumed to be 25 J/kg*K between 1090 and 1300K.

Above the alpha + beta to beta transformation temperature (about 1250K) and up to about 1320K, a constant value of 355.7 J/kg*K was reported by Deem and Eldridge (1967). This value agrees well with a value of 365.3 reported by Coughlin and King (1950) for pure beta zirconium. The standard error of

specific heat calculations made above 1300K is assumed to be 100 J/kg*K in the FRAPCON-3.5/FRAPTRAN-1.5 codes.

In addition to Zircaloy alloys, FRAPTRAN-1.5 has been modified to include specific heat calculations for ZrNb-1. These calculations are based on data collected at two different heating rates. Depending on the user input, specific heat calculations can be based on either the fast or the slow heating rate data. The data used to interpolate specific heat values for the ZrNb-1 alloy are presented in the following table. There is no standard error described for specific heat calculations based on these data sets.

			Standard Error	
Temperature (K)	Specific Heat Capacity (J/kg*K)	Source	MATPRO (J/kg*K)	FRAPCON-3 / FRAPTRAN (J/kg*K)
----------Alpha Phase----------				
300	281	Brooks and Stansbury	1.1	10
400	302	Brooks and Stansbury	1.1	10
640	331	Brooks and Stansbury	1.1	10
1090	375	Brooks and Stansbury	2.8	10
----------Beta Phase----------				
1093	502	Deem and Eldridge	10.7	25
1113	590	Deem and Eldridge	10.7	25
1133	615	Deem and Eldridge	10.7	25
1153	719	Deem and Eldridge	10.7	25
1173	816	Deem and Eldridge	10.7	25
1193	770	Deem and Eldridge	10.7	25
1213	619	Deem and Eldridge	10.7	25
1233	469	Deem and Eldridge	10.7	25
1248	356	Deem and Eldridge	10.7	25
2098	356	Coughlin and King	100	100
2099	356	Coughlin and King	100	100

Specific heat capacity database for Zircaloy-2, Zircaloy-4, ZIRLO, Optimized ZIRLO, and M5.

4.2.4 Emissivity

The subcode ZOEMIS returns the cladding surface emissivity, which is directly proportional to the radiant heat transfer from the cladding surface during an abnormal transient. The ZOEMIS model described in MATPRO is the same as the model used in FRAPCON-3.5 and FRAPTRAN-1.5.

When the cladding surface temperature has not exceeded 1500K, emissivities are modelled by the first 2 equations below. The first equation is used for oxide layers less than 3.88×10^{-6} m thick and the second one is used for oxide layers equal to or greater than 3.88×10^{-6} m thick. Both equations relate the hemispherical emissivity, ε1 (dimensionless), to the oxide layer thickness, d (m).

$$\varepsilon_1 = 0.325 + 0.1246 \; x \; 10^6 \, d \qquad d < 3.88 \times 10^{-6}$$

$$\varepsilon_1 = 0.808642 - 50.0\,d \qquad d > 3.88\text{x}10^{-6}$$

When the maximum cladding temperature has exceeded 1500K, emissivity is taken to be the larger of 0.325 and the result of the equation below. This equation relates the emissivity above 1500K, ε_2 (dimensionless), to ε_1 and the maximum cladding temperature, T (K).

$$\varepsilon_2 = \varepsilon_1 \exp\left[\frac{1500 - T}{300}\right]$$

4.2.5 Hardness

The subroutine CMHARD calculates Meyer hardness as a function of cladding temperature. Hardness is one of the parameters required for calculating fuel-to-cladding contact conductance. As the contact pressure between the two surfaces increases, the points of contact enlarge due to localized plastic deformation and the solid-to-solid thermal conductance is improved. The Meyer hardness is used by Ross and Stoute (1962) in their heat transfer correlation as an indication of the hardness of resistance to deformation of the softer (Zircaloy) material.

The same CMHARD subroutine is used in the MATPRO, FRAPCON-3.5, and FRAPTRAN-1.5 codes. However, FRAPTRAN-1.5 includes additional coding that ensures that the minimum hardness returned is $1.94\text{x}10^8$ N/m^2 (the highest temperature data point) and includes provisions for ZrNb-1.

In MATPRO, the Meyer hardness number is a measure of indentation hardness and is defined in conjunction with Meyer's law:

$$L = ad^n$$

where

L = load
d = the diameter of impression at the surface of a specimen in a static ball test
n = the Meyer work hardening coefficient
a = a material constant

The Meyer hardness number (MH) is defined as $4L/\pi d2$. Other hardness numbers are available (Brinell, Rockwell, etc.), and conversion from one to another is possible. However, the routine CMHARD was created to provide information required by the Ross and Stoute gap conductance model that includes a dependence on Meyer hardness.

Meyer hardness numbers for temperatures from 298 to 877K were taken from Peggs and Godin (1975). A regression analysis of the reciprocal of the Meyer hardness values versus the log of temperature was used to obtain the analytical expression used in CMHARD. The correlation used is given by:

$$MH = \exp\left\{2.6034x10^{1} + T\left\{-2.6394x10^{-2} + T\left[4.3502x10^{-5} + T\left(2.5621x10^{-8}\right)\right]\right\}\right\}$$

where

MH = Meyer hardness (N/m^2)
T = temperature (K)

4.2.6 Thermal expansion coefficient

The subroutine CTHEXP returns the axial and diametral components of thermal expansion in the cladding as a function of temperature. The model for cladding thermal expansion in the FRAPCON-3.5/FRAPTRAN-1.5 (FRAP) codes is different from the MATPRO model but provides similar predictions of expansion (< 6 percent). The data for the FRAP correlation used from room temperature to 1273K was taken from Mehan and Wiesinger (1961), Scott (1965), and Kearns (1965). Above 1273K, the coefficient of thermal expansion is the constant value of 9.7×10^{-6}, as recommended by Lustman and Kerze (1955). Between 1073 and 1273K (approximately the alpha-beta transition range for Zircaloy), the thermal expansion components are determined by linear interpolation.

The correlations used to calculate the axial and diametral components of thermal expansion in the cladding between room temperature and 1073K are presented below. Strain is given a function of temperature, T (°C).

$$\varepsilon_{axial} = -2.5060 \times 10^{-5} + 4.4410 \times 10^{-6} T$$
$$\varepsilon_{diametral} = -2.3730 \times 10^{-5} + 6.7210 \times 10^{-6} T$$

The correlations used to calculate the axial and diametral components of thermal expansion in the cladding above 1273K are presented below. Strain is given a function of temperature, T (°C).

$$\varepsilon_{axial} = -8.300 \times 10^{-3} + 9.70 \times 10^{-6} T$$
$$\varepsilon_{diametral} = -6.800 \times 10^{-3} + 9.70 \times 10^{-6} T$$

4.2.7 Young's modulus

Elastic moduli are required to relate stresses to strains. The elastic moduli are defined by the generalized form of Hooke's law as elements of the fourth rank tensor that relates the second rank stress and strain tensors below the yield point. In practice, cladding is frequently assumed to be an isotropic material. In such a case, only two independent elastic moduli are needed to describe the relation between elastic stress and strain: the Young's modulus and the shear modulus.

The subcodes CELMOD and CSHEAR are used in the MATPRO and the FRAPCON 3.5/FRAPTRAN-1.5 (FRAP) codes to determine the Young's modulus and the shear modulus, respectively. The tensor from which these moduli are derived is calculated by CELAST, which is included in MATPRO and determines the compliance matrix for isotropic cladding. However, CELAST is not used in the FRAP codes. The subcode CELAST would only be required if the Young's modulus and shear modulus for an anisotropic cladding is desired but the cladding is assumed to be isotropic.

4.2.8 CELMOD

The CELMOD subcode included in the FRAP codes differs only in form from the MATPRO version. For instance, the expression for Young's modulus in the alpha phase is presented below.

$$cel\,\mathrm{mod} = (1.088x10^{11} - 5.475x10^{7} * ctemp + c_1 * deloxy + c_3 * cwkf) / c_2$$

where

celmod = Young's modulus (Pa)
ctemp = cladding temperature (K)
deloxy = input average oxygen concentration excluding oxide layer (kg oxygen/kg Zircaloy) (hardwired to zero in FRAPCON-3.5/FRAPTRAN-1.5)
cwkf = input effective cold work (dimensionless less ratio of areas)

c_1, c_2, and c_3 are expressions that account for oxygen content, cold work, and fast neutron fluence respectively:

$$c_1 = \left(1.16x10^{11} + ctemp * 1.037x10^{8}\right) * 5.7015$$
$$c_2 = 1.0$$
$$c_3 = -2.6x10^{10}$$

For neutron fluences greater than $1x10^{22}$, c_2 is given by:

$$c_2 = 0.88 * \left(1 - \exp\left(- fnck / 1x10^{25}\right)\right) + \exp\left(- fnck / 1x10^{25}\right)$$

where

fnck = input effective fast fluence (n/m^2)

4.2.8.2 CSHEAR

The CSHEAR subcode included in the FRAP codes differs slightly from the MATPRO version. For instance, the expression for shear modulus in the alpha phase is presented below:

$$cshear = (4.04x10^{10} - 2.168x10^{7} * ctemp + c_1 * deloxy + c_3 * cwkf) / c_2$$

where

cshear = shear modulus (Pa)
ctemp = cladding temperature (K)
deloxy = input average oxygen concentration excluding oxide layer
cwkf = input effective cold work (dimensionless ratio of areas)

c_1, c_2, and c_3 are expressions that account for oxygen content, cold work, and fast neutron fluence, respectively:

$$c_1 = 7.07x10^{11} - ctemp * 2.315x10^{8}$$
$$c_2 = 1.0$$
$$c_3 = -0.867x10^{10}$$

For neutron fluences greater than $1x10^{22}$, c_2 is given by:

$$c_2 = 0.88 * \left(1 - \exp\left(- fnck / 1x10^{25}\right)\right) + \exp\left(- fnck / 1x10^{25}\right)$$

where

fnck = input effective fast fluence (n/m^2)

4.2.9 Poisson's ratio

This is calculated using ν=E/2G-1, where E and G are the Young's and shear moduli, respectively, calculated as described above by subroutines CELMOD and CSHEAR.

4.2.10 Yield strength

This has not been documented properly, but is calculated in CMLIMT. The line reads:

```
! Calculate yield strength
cyldst = (ag/(elmod**an))**(1.0d0/(1.0d0 - an))
```

with:

```
ag = ak * ((rstran/1.0d-03)**am)
```

with rstran the strain rate, ak (strength coefficient K) and am (strain rate hardening exponent m) calculated in CKMN, and elmod calculated in CELMOD.

The resulting calculation is equivalent to:

$$\sigma_y = \left(\frac{K}{E^n}\dot{\varepsilon}^m\right)^{\frac{1}{1-n}}$$

4.2.11 Mechanical behaviour model

The cladding deformation model in FRACAS-I is based on the following assumptions:

1. Incremental theory of plasticity.
2. Prandtl-Reuss flow rule.
3. Isotropic work hardening.
4. No low-temperature creep deformation of cladding.
5. Thin wall cladding (stress, strain, and temperature uniform through cladding thickness).
6. No axial slippage occurs at fuel-cladding interface when fuel and cladding are in contact.
7. Bending strains and stresses in cladding are negligible.
8. Axisymmetric loading and deformation of the cladding.

Deformation and stresses in the cladding in the open gap regime are calculated using a model which considers the cladding to be a thick cylindrical shell (stress at mid-wall) with specified internal and external pressures and a prescribed uniform temperature.

Calculations for the closed gap regime are made using a model which assumes that the cladding is a thin cylindrical shell with prescribed external pressure and a prescribed radial displacement of its inside surface. The prescribed displacement is obtained from the fuel thermal expansion model. Furthermore, because no slippage is assumed when the fuel and cladding are in contact, the axial expansion of the fuel is transmitted directly to the cladding. Hence, the change in axial strain in the shell is also prescribed.

Two additional models are used to calculate changes in yield stress with work hardening, given a uniaxial stress-strain curve. This stress-strain curve is obtained from the mechanical properties. The first model calculates the effective total strain and new effective plastic stress given a value of effective stress and the effective plastic strain at the end of the last loading increment. Depending on the work-hardened value of yield stress, loading can be either elastic or plastic, and unloading is constrained to occur elastically (Isotropic work hardening is assumed in these calculations).

The determination as to whether or not the fuel is in contact with the cladding is made by comparing the radial displacement of the fuel with the radial displacement that would occur in the cladding due to the prescribed external (coolant) pressure and the prescribed internal (fission and fill gas) pressure. The determination is expressed by the equation:

$$u_r^{fuel} \geq u_r^{clad} + \delta$$

where

δ = as-fabricated fuel-cladding gap size (m)

If the above equation is satisfied, the fuel is determined to be in contact with the cladding. The loading history enters into this determination by virtue of the permanent plastic cladding strains imposed in the cladding by the cladding loads.

If the fuel and cladding displacements are such that the above equation is not satisfied, the fuel-cladding gap has not closed during the current loading step and the open gap solution is used.

If the fuel and cladding have come into contact during the current loading increment, radial continuity at the contact interface requires that:

$$u_r^{clad} = u_r^{fuel} - \delta$$

while in the axial direction the assumption is made that no slippage occurs between the fuel and cladding. This state is referred to as PCMI or “lockup”.

Note that only the additional strain which occurs in the fuel after PCMI has occurred is transferred to the cladding. Thus, if $\varepsilon_{z,o}^{clad}$ is the axial strain in the cladding just prior to contact and $\varepsilon_{z,o}^{fuel}$ is the corresponding axial strain in the fuel, then the no-slippage condition in the axial direction becomes

$$\varepsilon_z^{clad} - \varepsilon_{z,o}^{clad} = \varepsilon_z^{fuel} - \varepsilon_{z,o}^{fuel}$$

The mechanical properties of fuel rod Zircaloy cladding are known to change with irradiation because of damage from the fast neutron fluence. The changes are similar to cold-working the material because dislocation tangles are created that tends to both strengthen and harden the cladding while decreasing the ductility. In addition to the fast fluence effects, excess hydrogen in the Zircaloy, in the form of hydrides, may affect the mechanical properties.

An analysis of recent data from mechanical testing of irradiated Zircaloy was conducted as part of the development work for FRAPCON-3 and revised equations for use in FRAPCON-3 and FRAPTRAN routines were then generated (Geelhood et al., 2008). The following summarizes the mechanical property equations.

Three models account for the high fast neutron fluence levels, temperature, and strain rate in the cladding. Those models are

a) the strength coefficient in CKMN,

b) the strain hardening exponent in CKMN,

c) the strain rate exponent in CKMN.

4.2.11.1 Strength coefficient, K

The strength coefficient, K, is a function of temperature, fast neutron fluence, cold work, and alloy composition. The strength coefficient has not been found to be a function of hydrogen concentration. The models for the strength coefficients of Zircaloy-2 and Zircaloy-4 are given below.

$$K = K(T)\cdot(1+K(CW)+K(\Phi))/K(Zry)$$

where

$$K(T) = 1.17628\times10^{9} + 4.54859\times10^{5}T - 3.28185\times10^{3}T^{2} + 1.72752\cdot T^{3} \qquad T < 750\text{K}$$

$$K(T) = 2.522488\times10^{6}\exp\left(\frac{2.8500027\times10^{6}}{T^{2}}\right) \qquad 750\text{K} < T < 1090\text{K}$$

$$K(T) = 1.841376039\times10^{8} - 1.4345448\times10^{5}T \qquad 1090\text{K} < T < 1255\text{K}$$

$$K(T) = 4.330\times10^{7} - 6.685\times10^{4}T + 3.7579\times10^{1}T^{2} - 7.33\times10^{-3}T^{3} \qquad 1255\text{K} < T < 2100\text{K}$$

$$K(CW) = 0.546\cdot CW$$

$$K(\Phi) = (-0.1464 + 1.464\times10^{-25}\Phi)\,f(CW,T) \qquad \Phi < 0.1\times10^{25}\ \text{n/m}^2$$

$$K(\Phi) = 2.928\times10^{-26}\Phi \qquad 0.1\times10^{25}\text{n/m}^2 < \Phi < 2\times10^{25}\ \text{n/m}^2$$

$$K(\Phi) = 0.53236 + 2.6618\times10^{-27}\Phi \qquad 2\times10^{25}\ \text{n/m}^2 < \Phi < 12\times10^{25}\ \text{n/m}^2$$

$$f(CW,T) = 2.25\exp(-20\cdot CW)\cdot\min\left[1,\exp\left(\frac{T-550}{10}\right)\right]+1$$

K(Zry) = 1 for Zircaloy-4
K(Zry) = 1.305 for Zircaloy-2
T = temperature (K)
CW = cold work, dimensionless ratio of areas (valid from 0 to 0.75)
Φ = fast neutron fluence, n/m² (E>1MeV)

The effective cold work and fast neutron fluence used to calculate the strength coefficient, K, can be reduced by annealing if the time or temperature, or both, are high enough. FRAPTRAN uses the MATPRO (Hagrman et al., 1981) model, CANEAL, to calculate the effective cold work and fast neutron fluence at each time step using the following equations.

$$CW_i = CW_{i-1} \exp\left[-1.504(1 + 2.2\times10^{-25}\phi_{i-1})(t) \exp\left(\frac{-2.33\times10^{18}}{T^6} \right) \right]$$

$$\phi_i = \frac{10^{20}}{2.49\times10^{-6}(t)\exp\left(\frac{-5.35\times10^{23}}{T^8} \right) + \frac{10^{20}}{\phi_{i-1}}}$$

where

CW_{i-1}, and CW_i	=	the effective cold work for strength coefficient at the start and end of the time step, respectively (dimensionless ratio of areas)
ϕ_i, and ϕ_{i-1}	=	effective fast neutron fluence for strength coefficient at the start and end of the time step, respectively (n/m^2)
t	=	time step size (s)
T	=	cladding temperature (K)

4.2.11.2 Strain-hardening exponent, n

The strain-hardening exponent, n, is a function of temperature, fast neutron fluence, and alloy composition. The strain-hardening exponent has not been found to be a function of hydrogen concentration. The models for the strain-hardening exponents of Zircaloy-2 and Zircaloy-4 are given below.

$$n = n(T) \cdot n(\Phi) / n(Zry)$$

where

$$n(T) = 0.11405 \qquad T < 419.4K$$

$$n(T) = -9.490\times10^{-2} + 1.165\times10^{-3}T - 1.992\times10^{-6}T^2 + 9.588\times10^{-10}T^3 \qquad 419.4K < T < 1099.0772K$$

$$n(T) = -0.22655119 + 2.5\times10^{-4}T \qquad 1099.0772K < T < 1600K$$

$$n(T) = 0.17344880 \qquad > 1600K$$

$$n(\Phi) = 1.321 + 0.48\times10^{-25}\Phi \qquad \Phi < 0.1\times10^{25}\ n/m^2$$

$$n(\Phi) = 1.369 + 0.096\times10^{-25}\Phi \qquad 0.1\times10^{25}\ n/m^2 < \Phi < 2\times10^{25}\ n/m^2$$

$$n(\Phi) = 1.5435 + 0.008727\times10^{-25}\Phi \qquad 2\times10^{25}\ n/m^2 < \Phi < 7.5\times10^{25}\ n/m^2$$

$$n(\Phi) = 1.608953 \qquad \Phi > 7.5\times10^{25}\ n/m^2$$

n(Zry) = 1 for Zircaloy-4
n(Zry) = 1.6 for Zircaloy-2
T = temperature (K)
Φ = fast neutron fluence (n/m^2) (E>1MeV)

The effective fast neutron fluence used to calculate the strain-hardening exponent, n, can be reduced by annealing if the time or temperature, or both, are high enough. FRAPCON-3 uses the MATPRO (Hagrman et al., 1981) model, CANEAL, to calculate the fast neutron fluence at each time step using the following equations.

$$\phi_i = \frac{10^{20}}{2.49\times10^{-6}(t)\exp\left(\frac{-5.35\times10^{23}}{T^8}\right)+\frac{10^{20}}{\phi_{i-1}}}$$

where

ϕ_i, and ϕ_{i-1}	=	effective fast neutron fluence for strain hardening exponent at the start and end of the time step, respectively (n/m^2)
t	=	time step size (s)
T	=	cladding temperature (K)

4.2.11.3 Strain rate exponent

The strain rate exponent, m, is given by a function of temperature only as described in the equation below:

$$m = 0.015 \qquad T < 750K$$
$$m = 7.458\times10^{-4}T - 0.544338 \qquad 750K < T < 800K$$
$$m = 3.24124\times10^{-4}T - 0.20701 \qquad T > 800K$$

where

m	=	strain rate exponent
T	=	temperature (K)

The impact of the strain rate exponent on yield stress is to increase the yield strength with increasing strain rate, but the effect is not large. For example, increasing the strain rate from 10^{-4}/s to 1.0/s will increase the yield strength by about 15 percent.

4.2.11.4 Assembled model

Tensile strength, yield strength, and strain are calculated using the same relationships in the CMLIMT subroutine. The true ultimate strength is calculated using

$$\sigma = K\left(\frac{\dot{\varepsilon}}{10^{-3}}\right)^m \varepsilon_{p+e}^n$$

where

σ	=	true ultimate strength (MPa)
K	=	strength coefficient (MPa)
$\dot{\varepsilon}$	=	strain rate (dimensionless)
m	=	strain rate sensitivity constant (dimensionless)
$\varepsilon_{p+\varepsilon}$	=	true strain at maximum load (dimensionless)
n	=	strain hardening exponent (dimensionless)